Conference paper

Lucas L. R. Vono, Camila C. Damasceno, Jivaldo R. Matos, Renato F. Jardim, Richard Landers, Sueli H. Masunaga and Liane M. Rossi*

Separation technology meets green chemistry: development of magnetically recoverable catalyst supports containing silica, ceria, and titania

https://doi.org/10.1515/pac-2017-0504

Abstract: Magnetic separation can be considered a green technology because it is fast, efficient, consumes low energy, and minimizes the use of solvents and the generation of waste. It has been successfully used in laboratory scale to facilitate supported catalysts' handling, separation, recovery, and recycling. Only few materials are intrisically magnetic, hence the application of magnetic materials as catalyst supports has broaden the use of magnetic separation. Iron oxides, silica-coated iron oxides, and carbon-coated-cobalt are among the most studied catalyst supports; however, other metal oxide coatings, such as ceria and titania, are also very interesting for application in catalysis. Here we report the preparation of magnetically recoverable magnetic supports containing silica, ceria, and titania. We found that the silica shell protects the iron oxide core and allows the crystalization of ceria and titania at high temperature without compromising the magnetic properties of the catalyst supports.

Keywords: catalyst support; ceria; ICGC-6; magnetic separation; magnetite; titania.

Introduction

Catalytic routes applied for the synthesis of complex organic molecules is highly desired but yet hindered by both high costs and difficulties in catalyst separation and recycling. For almost any manufacturing process using suspended or soluble catalysts, recovery of the spent catalyst from the product streams is a major concern [1]. The choice of the separation process is determined by the nature of the catalyst material and the time and energy consumed. Magnetic separation generally offers high efficiency and specificity when compared with equivalent centrifugation, filtration, liquid-liquid extraction, or chromatographic methods [1]. The possibility to use of magnetic separation is not always obvious, though if some part of a mixture is intrinsically magnetic (Ni, Co, Fe), then magnetic separation is often the best choice [2]. Each separation method has its own limitations of cost, efficiency, or generation of secondary waste, but magnetic separation meets many criteria to be considered a green technology. Magnetic separation generally offers the following advantages:

Article note: A collection of invited papers based on presentations at the 6th International IUPAC Conference on Green Chemistry (ICGC-6), Venice (Italy), 4–8 September 2016.

***Corresponding author: Liane M. Rossi,** Department of Fundamental Chemistry, Institute of Chemistry, University of São Paulo, 05508-000 São Paulo, Brazil, e-mail: lrossi@iq.usp.br
Lucas L. R. Vono, Camila C. Damasceno and Jivaldo R. Matos: Department of Fundamental Chemistry, Institute of Chemistry, University of São Paulo, 05508-000 São Paulo, Brazil
Renato F. Jardim: Institute of Physics, University of São Paulo, 05315-970 São Paulo, Brazil
Richard Landers: Institute of Physics Gleb Wataghin, State University of Campinas, Campinas 13083-859, Brazil
Sueli H. Masunaga: Physics Department, Centro Universitário FEI, 05508-090, São Bernardo do Campo, Brazil

- fast and efficient separation
- specific for separation of the magnetic component only
- low energy consumption (magnet, electromagnet)
- easy catalyst recycling – catalyst is kept inside the reactor
- minimizes catalyst loss
- minimizes exposure to air
- easy catalyst handling under inert condition
- easy sampling and product isolation under inert condition
- solvent-free process
- minimizes the prodution of waste
- applicable for any volume – possible to scale-up
- simple design
- applicable for any kind of catalysts (molecular, enzyme, metal, etc.)

As only few materials are intrisically magnetic, the application of magnetic separation to non-magnetic catalysts has been conceived by using magnetic materials as catalyst supports. Magnetic nanoparticles (MNPs), e.g. magnetite (Fe_3O_4), maghemite (Fe_2O_3), cobalt, etc., have attracted attention as catalyst supports because they provide fast separation under an applied magnetic field and easy redispersion in the absence of an applied magnetic field. Among the MNPs, magnetite can be highlighted as one of the most used magnetic supports, because they are easilly prepared by low-cost methodologies [3]. Many strategies for the immobilization of different type of catalysts on MNPs, such as metal complexes, metal or oxide nanoparticles, enzymes, or organocatalysts have been reported [2, 4, 5]. The design of magnetically recoverable catalysts consists in the functionalization of MNPs surfaces before the attachment of the catalyst to the magnetic phase [1, 3]. Many research groups have chosen to use MNPs coated with another material [3], typically silica [6] or carbon [7–9]. Coating the MNP surface is a strategy to protect the magnetic material against oxidation and aggregation, but it also facilitates the immobilization of catalysts through covalent attachment or electrostatic interactions [3, 10]. The coating of MNPs with other oxides, such as titania, alumina, and ceria, is highly desired to expand the use of MNPs as catalyst supports. Here we report the design of magnetically recoverable magnetic supports containing silica, ceria, and titania.

Development of magnetic supports

Silica-coated magnetite nanoparticles ($Fe_3O_4@SiO_2$) were obtained by the reverse microemulsion method reported elsewhere [11]. This method was chosen due to the high quality of the magnetic materials – spherically coated with silica – obtained with this methodology. We have been using this material as a catalyst support for metal nanoparticles [2, 12–18], metal complexes [19], and enzymes [20, 21] to perform a large scope of reactions. All the reactions have been performed at relatively mild conditions (<373 K) because the stability of the $Fe_3O_4@SiO_2$ material upon thermal treatment has never been studied in detail. Cheng et al. [22] reported that the silica-coated magnetite can be calcined, but they did not present a proper characterization of the calcined material. The materials obtained by the reverse microemulsion process may contain residual organic matter, primarly from the surfactant, in the silica shell. If the material is submitted to thermal treatment, these organic residues will be removed and an increase of the surface area is expected. However, the heat treatment of the material at high temperatures might result in changes in the magnetic properties due to magnetite oxidation and lead to other structural changes that still have to be determined.

Silica-coated magnetite: tuning the silica shell thickness

Initially, the effect of reaction time in the thickness of the silica shell was studied. From a typical microemulsion reaction, samples were collected after 2, 6, 12, 24, and 48 h reaction time. The silica-coated mag-

netite particles were purified following the same steps described before and their average size accessed by transmission electron microscopy (TEM) characterization. The average particle size was determined to be 20.1 ± 1.3, 28.0 ± 2.0, 31.2 ± 1.0, 33.8 ± 1.2, and 34.7 ± 1.2 nm, respectively. The sample, isolated after 2 h, shows a pearl-necklace structure due to an excess of non-reacted silica precursor, which undergoes hydrolysis and precipitation during the washing process. The sample, isolated after 6 h, exbibited the core-shell strucuture and the solid could be isolated without aggregation. This material was used for further studies.

Silica-coated magnetite: thermal stability

The thermal behavior of uncoated Fe_3O_4 NPs and Fe_3O_4@SiO_2 (prepared in 6 h), which contains a silica shell of about 10 nm, were studied by thermogravimetry/derivative thermogravimetry (TG/DTG) under dynamic air atmosphere. The two events of mass loss observed for Fe_3O_4@SiO_2 in Fig. 1a are related to water removal ($\Delta m = 7.9\,\%$, $T_{peak\ DTG} = 355$ K) and to the thermal decomposition of the surfactant IGEPAL CO-520 ($\Delta m = 5.1\,\%$, $T_{peak\ DTG} = 696$ K), respectively. The thermal decomposition temperature for the free surfactant is coincident with the temperature of the second event of mass loss observed, which is absent in the TG/DTG curves of the uncoated magnetite sample. Using the TG data, we have chosen to performe a calcination step under a static atmosphere of air at 773 K for 2 h with an initial heating rate of 20 K min^{-1}. A TG/DTG curves obtained with the calcination conditions (Fig. 1b) showed similar mass loss ($\Delta m = 5.6\,\%$ $T_{peak\ DTG} = 692$ K) attributed to organic residues removal. The water content in the sample can be slightly different and is attributed to the drying conditions. The amount of organic residues may also vary according to the surfactant removal efficiency in the washing procedure.

The surface area of the material obtained after calcination (and removal of the organic surfactants used in the microemulsion process) enhanced substantially from 18 to 111 $m^2\ g^{-1}$, but the core-shell morphology and the size of the silica nanospheres were preserved. Figure 2 exhibits the TEM micrograph of the material "as-prepared" and after the calcination process. The average size for the calcined material was determined to be 28.1 ± 1.2 nm. A careful inspection of the figure indicates that the morphology and size of the heat treated sample are quite similar to the as-prepared sample, with no clear damage to the material. The crystallinity and the phase purity of the as-prepared and calcined Fe_3O_4 and Fe_3O_4@SiO_2 materials were further characterized by X-ray powder diffraction (XRD) (Fig. 3). The XRD pattern of Fe_3O_4 NPs and Fe_3O_4@SiO_2 samples revealed diffraction peaks at 30.02°, 35.40°, 43.45°, 53.75°, 57.25° and 62.95° corresponding to the indexed planes of cubic Fe_3O_4 (2 2 0), (3 1 1), (4 0 0), (4 2 2), (5 1 1) and (4 4 0), according to the crystallographic data (ICSD #084611). The XRD pattern of calcined Fe_3O_4@SiO_2 samples preserved the same diffraction peaks

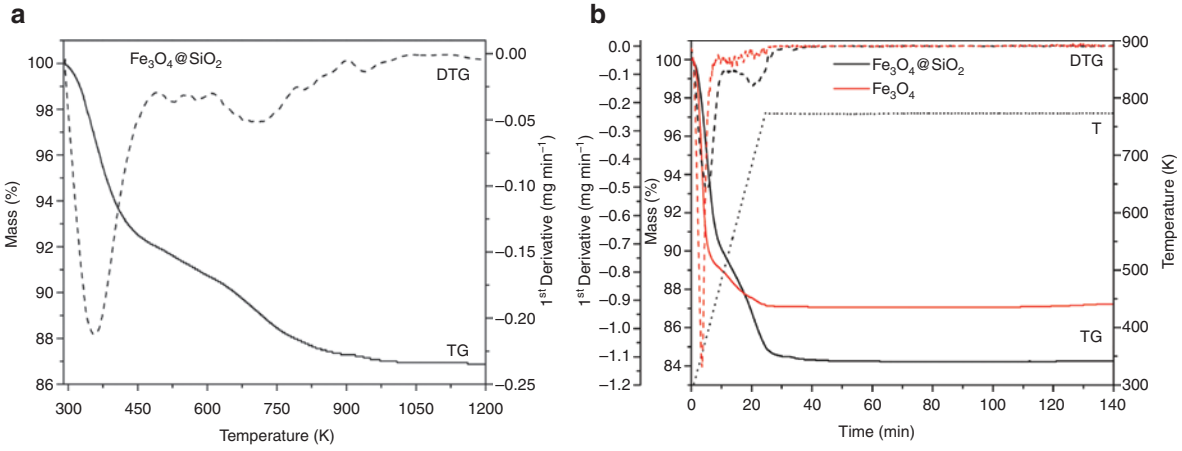

Fig. 1: TG (solid) and DTG (dashed) curves for Fe_3O_4@SiO_2 (black) and Fe_3O_4 NPs (red) with heating rate 20 K min^{-1} (a) until 1200 K and (b) isothem at 773 K for 2 h with dynamic atmosphere of air.

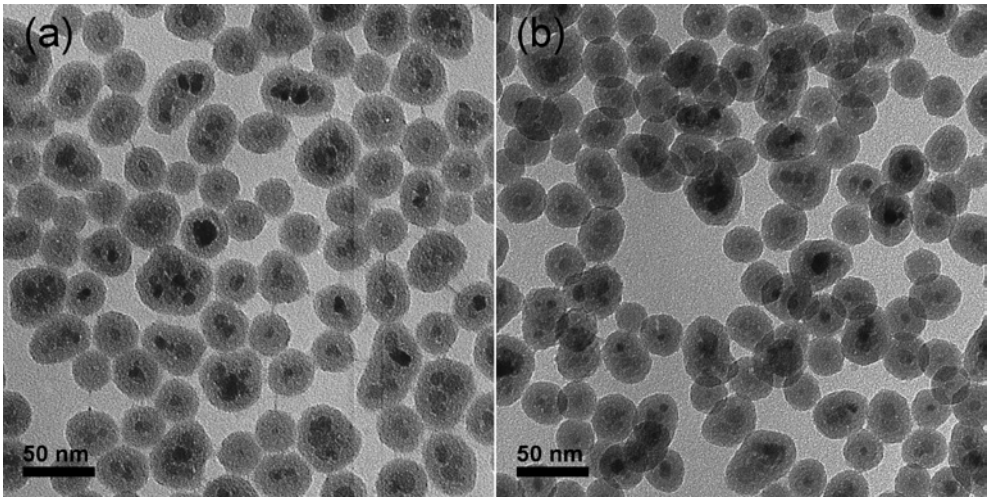

Fig. 2: Micrographs obtained by TEM of Fe_3O_4@SiO_2 materials (a) as-prepared and (b) after calcination.

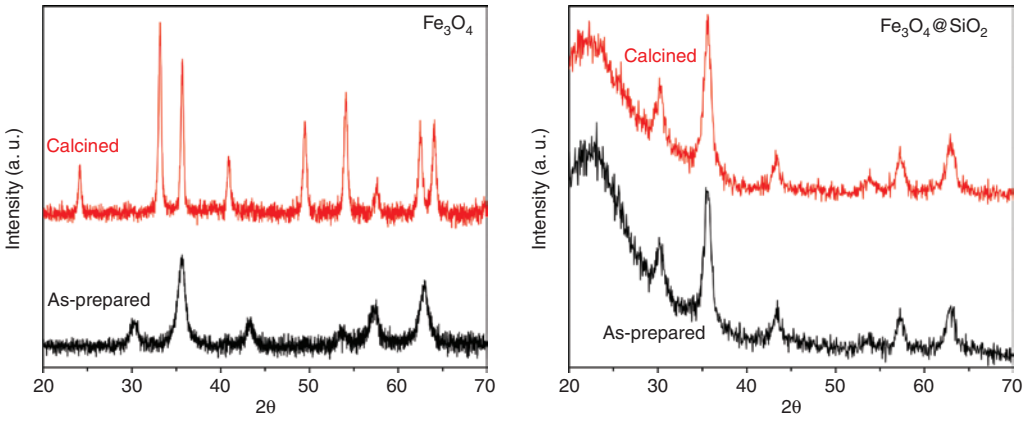

Fig. 3: XRD pattern of Fe_3O_4 (left) and Fe_3O_4@SiO_2 (right) as-prepared (black) and calcined (red).

corresponding to magnetite. However, the XRD pattern of uncoated Fe_3O_4 NPs calcined under similar conditions revealed diffraction peaks at 24.10°, 33.16°, 35.68°, 40.88°, 49.50°, 54.12°, 57.64°, 62.46° and 64.08° corresponding to indexed planes of rhombohedral α-Fe_2O_3 (0 1 2), (1 0 4), (1 1 0), (1 1 3), (0 2 4), (1 1 6), (0 1 8), (2 1 4) and (3 0 0) (ICSD #082904). These results indicate that the thermal treatment had little influence in the magnetic core crystal phase coated by silica, detectable by this technique, but resulted in oxidation of the uncoated Fe_3O_4 NPs into α-Fe_2O_3 particles with larger sizes. These results demonstrated an enhanced thermal stability of the silica-coated magnetite nanoparticles when compared to bare magnetite. The thermal stability is further investigated by magnetic measurements.

The magnetization M as a function of the applied magnetic field at 2 and 300 K, $M(H)$, and cycles of zero field cooled (ZFC) and field cooled (FC), measured under $H = 50$ Oe and in a large range of temperature, were performed to evaluate the magnetic properties of Fe_3O_4@SiO_2, as illustrated in Fig. 4. No significant changes were observed in $M(H)$ and ZFC/FC curves for Fe_3O_4@SiO_2 before (as-prepared) and after calcination. The two samples show typical characteristics of superparamagnetic particles: ZFC curves presenting a maximum related with the blocking temperature (T_B) of the system, reversible $M(H)$ curves above T_B with negligible coercive field and remanent magnetization (Fig. 4a) and curves presenting magnetic hysteresis below T_B (Fig. 4a inset). The saturation magnetization (Ms) was 82 and 79 emu g^{-1} for as-prepared and calcined Fe_3O_4@SiO_2 samples, respectively. In addition, the magnetic size distributions ($\langle d \rangle \sim 6$ nm and $\sigma = 0.4$)

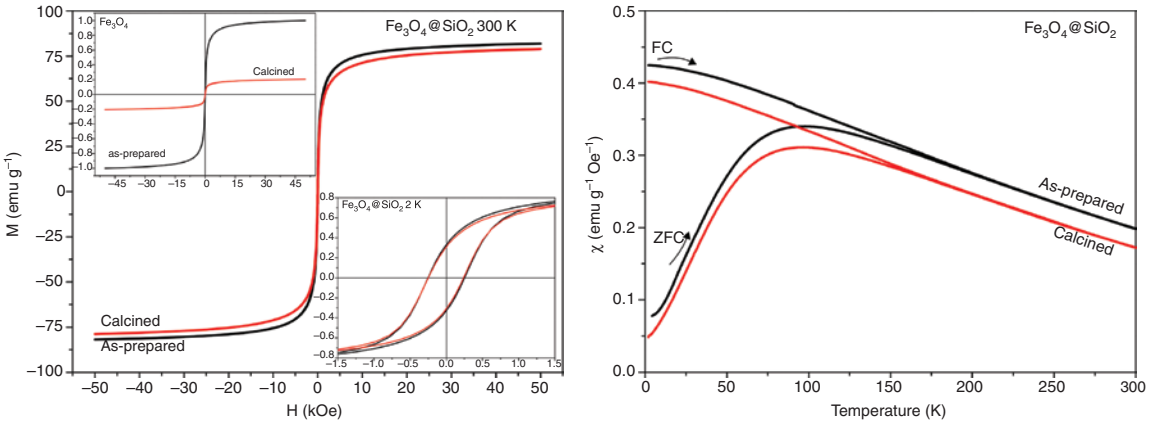

Fig. 4: Magnetization as a function of applied magnetic field measured at 300 K (left) and at 2 K (bottom inset) for as-prepared (black) and calcined (red) Fe_3O_4@SiO_2 and Fe_3O_4 (top inset). Magnetic susceptibility as function of temperature (right), measured under ZFC and FC conditions applying a magnetic field of $H = 50$ Oe for as-prepared (black) and calcined (red) Fe_3O_4@SiO_2. The results were corrected to magnetic mass and inset data is normalized.

estimated from the Langevin function fitted to $M(H)$ curves, a procedure found elsewhere [23], are also similar for both samples. Therefore, the magnetic core is preserved after thermal treatment. Figure 4b demonstrates that the ZFC magnetic susceptibilities reach their maximum at the same temperature for both as-prepared and calcined samples, indicating that the average blocking temperatures were found to remain essentially unchanged after the thermal treatment, further suggesting that the magnetic cores did not sinter upon heating. Contrarily, the calcination of uncoated Fe_3O_4 NPs drastically affected their magnetic properties. The M_S of bare Fe_3O_4 NPs decreased by nearly 80 % after calcination (air at 773 K for 2 h) (Fig. 4a inset), which may be due to the oxidation of Fe_3O_4 into α-Fe_2O_3 that typically exhibits a much lower Ms ~2 emu g^{-1}. Hence, we have observed an enhanced thermal stability of the silica-coated magnetite nanoparticles when compared to uncoated magnetite. The silica shell provides an extra protection to the magnetic core, suppressing the oxidation process, as evidenced by the preserved magnetic properties before and after the thermal treatment.

Post-coating process: magnetic supports containing ceria, titania and other oxides

Silica is a very versatile catalysts support; however, other metal oxides, such as ceria and titania, are also very interesting for application in the field of catalysis. The oxygen storage and release properties of ceria are crucial for various catalytic reactions, including those in exhaust catalysts. Our first attempt to prepare ceria-coated magnetite by the substitution of tetraethylortosilicate by ammonium cerium(IV) nitrate in the microemulsion process failed. Many other attempts to coating the magnetic core with ceria, titania, and alumina have lead to a fast precipitation process on the microemulsion system. The uncontrolled hydrolysis and condensation of such precursors and the lack of control of the material's morphology is still a problem to overcome. Moreover, the crystallization of ceria and other oxides occurs at high temperature and it can be a problem for uncoated magnetite nanoparticles. Taking advantage of the thermal stability of the silica-coated magnetite nanoparticles (see results above), we further explored the post-coating of Fe_3O_4@SiO_2 with different oxides. The deposition of ceria on the surface of the silica shell was performed by the wetness impregnation and thermal decomposition of ammonium cerium(IV) nitrate at 773 K for 2 h under static air atmosphere. The TEM micrograph of the material obtained after calcination revealed the presence of ceria nanoparticles of 2.6 ± 0.4 nm well distributed on the silica surface (Fig. 5a). The morphology of the core-shell silica coated magnetite was preserved. The XRD pattern of Fe_3O_4@SiO_2-CeO_2 revealed diffraction peaks at 28.75°, 33.10°, 47.80°, 56.35° corresponding to indexed planes of cubic CeO_2 (1 1 1), (2 0 0), (2 2 0) and (3 1 1) (ICSD #072155), additionally to diffraction peaks attributed to Fe_3O_4 (Fig. 5b).

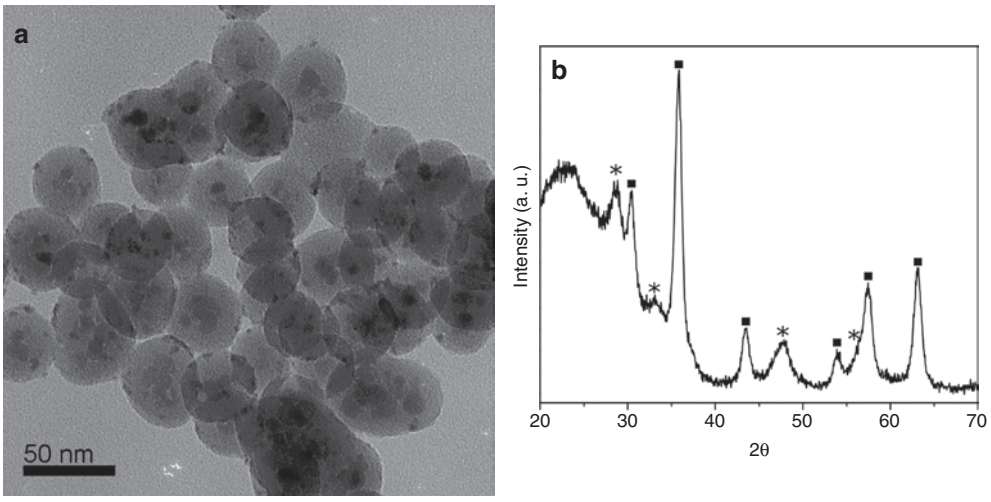

Fig. 5: (a) Micrograph obtained by TEM of Fe_3O_4@SiO_2-CeO_2. (b) XRD pattern of FFSiCe. The peaks attributed to magnetite are indicated with ■ and to ceria with *.

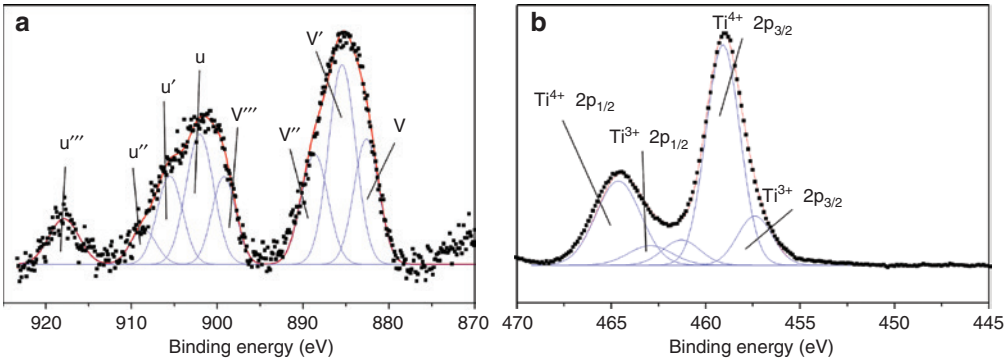

Fig. 6: XPS spectrum for (a) Ce 3d core level obtained with Fe_3O_4@SiO_2-CeO_2 and for (b) Ti 2p obtained with Fe_3O_4@SiO_2-TiO_2.

The deposition of small CeO_2 particles was also demonstrated by X-ray photoelectron spectrocopy (XPS). The XPS spectrum of the calcined Fe_3O_4@SiO_2 shows two O 1s components at binding energy (BE) 533.0 and 530.3 eV, attributed respectively to bulk SiO_2 and to surface hydroxyl groups, although, the latter is often observed in several oxides. The XPS spectrum for Fe_3O_4@SiO_2-CeO_2 showed an increase in the O 1s component at BE 530.7 eV, a feature attributed to the occurrence of CeO_2 [24]. There is an increase of 2.1 eV, compared to pure CeO_2 as a consequence of the decrease in the basicity of small CeO_2 particles. The Ce 3d XPS spectrum (Fig. 6a) showed eight components and, as described by Burroughs et al. [25] the components u, u″, and u‴ (903.26, 909.21, and 917.87 eV) and v, v″, and v‴ (882.63, 888.44, and 900.03 eV) are associated with Ce^{4+} 3d and the components v′ (885.33 eV) and u′ (906.30 eV) are attributed to Ce^{3+} 3d. As a result of the low content of Ce, the components v_0 and u_0 were not observed [26].

Titania has also received attention as a catalyst support that possesses good mechanical resistance, strong metal support interaction, chemical stability, and acid-base property and high potential in photocatalyst-related applications [27]. The deposition of titania on the surface of Fe_3O_4@SiO_2 was obtained following a different method [28]. The hydrolysis of titanium(IV) isopropoxide resulted in the formation of small particles and/or shell on the Fe_3O_4@SiO_2 surface that were characterized by TEM/EDS (Fig. 7) and XPS (Fig. 6b), but were not detectable by XRD. The HRTEM analysis of the small particles presented on the Fe_3O_4@SiO_2 surface resulted in an interplanar distance of 3.71 Å that corresponds to the (1 0 1) Bragg plane of anatase phase of TiO_2 [29]. The deposition of TiO_2 was also confirmed by XPS data (Fig. 6b). The Ti 2p doublet is assigned to Ti 2p3/2 and to Ti 2p1/2 at lower and higher energy, respectively. The Ti 2p XPS spectrum was fitted into two

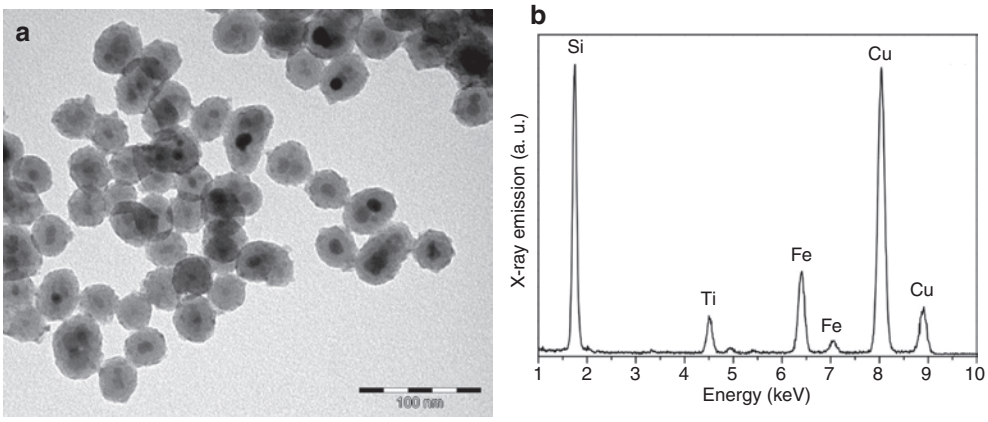

Fig. 7: (a) Micrograph obtained by TEM of Fe_3O_4@SiO_2-TiO_2 and (b) energy dispersive X-ray spectroscopy (EDS) analysis.

components for Ti^{4+} (464.63 and 459.09 eV) and Ti^{3+} (462.93 and 457.40 eV) species, which agreed with Ti^{4+} in pure anatase TiO_2 form [30]. The two Ti^{3+} peaks and the peak separation for Ti^{4+} and Ti^{3+} agreed with the reported values in the literature [31]. The peak at 461.3 eV is related to the X-ray emission source. The deposition of CeO_2 and TiO_2 was performed using ammonium cerium(IV) nitrate and titanium(IV) isopropoxide, and the presence of Ce^{3+} and Ti^{3+} is an consequence of the long time X-ray irradiation [32].

Concluding remarks

We were able to demonstrate the versatility of the post-coating process for the decoration of silica-coated magnetite nanoparticles with other inorganic oxides for the preparation of novel magnetically recoverable catalyst supports. The well-known reverse microemulsion methodology used for the preparation of high quality and size controlled silica-coated magnetite did not apply for the direct coating of magnetite with other oxides such as ceria and titania. Moreover, we have found that the pre-coating with a uniform layer of silica provides thermal resistant magnetic materials, which allows for thermal treatment without depleting the magnetic properties of the magnetic core. The deposition and crystallization of ceria and titania nanoparticles on the surface of silica-coated magnetite was obtained by very simple protocols. The post-coating of silica-coated magnetite with alumina and magnesia were also obtained, thus demonstrating that this is an efficient method to obtain magnetically recoverable catalyst supports containing different metal oxides and surface properties. All materials presented here are easily separated from complex mixtures by means of magnetic separation.

Experimental

Synthesis of magnetic supports

The magnetic support Fe_3O_4@SiO_2 was prepared by a microemulsion process reported elsewhere [12]. The influence of reaction time on the silica layer was studied by taking aliquots with 2, 6, 12, 24, and 48 h. The material was precipitated with methanol and separated by centrifugation. The solid was washed with two portions of ethanol followed by centrifugation and dried in air. The calcination procedure was performed under a static atmosphere of air at 773 K for 2 h (heating rate of 20 K min^{-1}). The post-coating with ceria was performed by dispersing 100 μg Fe_3O_4@SiO_2 in 4 mL ethanol and addition of 8 μg ammonium cerium(IV) nitrate, after 2 h, under magnetic stirring. The mixture was kept under magnetic stirring for another 20 h

before removing the solvent under vaccum. The obtained solid was thermally treated at 773 K for 2 h under static air atmosphere. The resulting material was denoted as Fe_3O_4@SiO_2-CeO_2. The post-coating with titania was performed by a modification of the method described by Güttel et al. [28] for the preparation of gold yolk-shell material. Initially, 200 µg Fe_3O_4@SiO_2 and 90 µL titanium(IV) isopropoxide solution (80 % in 1-butanol) were dispersed in Brij-30 solution (0.4 mmol L^{-1}, in 30 mL ethanol) under magnetic stirring. After 20 h, the solid was magnetically separated and washed with three portions of 15 mL ethanol. The obtained material was calcined under static air atmosphere at 773 K for 2 h. The resulting material was denoted as Fe_3O_4@SiO_2-TiO_2.

Acknowledgments: The authors are grateful for the financial support of FAPESP (Grants No. 2013/07296-2, 2014/19245-6, 2008/02878-5, 2012/08691-0, 2014/15159-8) and CNPq. The authors thank Prof. Pedro K. Kiyohara for TEM analysis. LLR Vono thanks FAPESP for his PhD fellowship (2010/11102-0).

References

[1] R. B. N. Baig, R. S. Varma. Magnetically retrievable catalysts for organic synthesis. *Chem. Commun.* **49**, 752 (2013).
[2] L. M. Rossi, N. J. S. Costa, F. P. Silva, R. Wojcieszak. Magnetic nanomaterials in catalysis: advanced catalysts for magnetic separation and beyond. *Green Chem.* **16**, 2906 (2014).
[3] D. Wang, D. Astruc. Fast-growing field of magnetically recyclable nanocatalysts. *Chem. Rev.* **114**, 6949 (2014).
[4] S. Shylesh, V. Schunemann, W. R. Thiel. Magnetically separable nanocatalysts: bridges between homogeneous and heterogeneous catalysis. *Angew. Chem.-Int. Ed.* **49**, 3428 (2010).
[5] V. Polshettiwar, R. Luque, A. Fihri, H. Zhu, M. Bouhrara, J.-M. Bassett. Magnetically recoverable nanocatalysts. *Chem. Rev.* **111**, 3036 (2011).
[6] D. K. Yi, S. S. Lee, J. Y. Ying. Synthesis and applications of magnetic nanocomposite catalysts. *Chem. Mater.* **18**, 2459 (2006).
[7] Z. Wang, P. Mao, N. He. Synthesis and characteristics of carbon encapsulated magnetic nanoparticles produced by a hydrothermal reaction. *Carbon* **44**, 3277 (2006).
[8] X. Dong, H. Chen, W. Zhao, X. Li, J. Shi. Synthesis and magnetic properties of mesostructured gamma-Fe_2O_3/carbon composites by a Co-casting method. *Chem. Mater.* **19**, 3484 (2007).
[9] Z. H. Wang, C. J. Choi, B. K. Kim, J. C. Kim, Z. D. Zhang. Characterization and magnetic properties of carbon-coated cobalt nanocapsules synthesized by the chemical vapor-condensation process. *Carbon* **41**, 1751 (2003).
[10] Y. Zhu, L. P. Stubbs, F. Ho, R. Liu, C. P. Ship, J. A. Maguire, N. S. Hosmane. Magnetic nanocomposites: a new perspective in catalysis. *ChemCatChem* **2**, 365 (2010).
[11] M. J. Jacinto, P. K. Kiyohara, S. H. Masunaga, R. F. Jardim, L. M. Rossi. Recoverable rhodium nanoparticles: synthesis, characterization and catalytic performance in hydrogenation reactions. *Appl. Catal. A Gen.* **338**, 52 (2008).
[12] L. M. Rossi, M. A. S. Garcia, L. L. R. Vono. Recent advances in the development of magnetically recoverable metal nanoparticle catalysts. *J. Braz. Chem. Soc.* **23**, 1959 (2012).
[13] L. M. Rossi, L. L. R. Vono, M. A. S. Garcia, T. L. T. Faria, J. A. Lopez-Sanchez. Screening of soluble rhodium nanoparticles as precursor for highly active hydrogenation catalysts: the effect of the stabilizing agents. *Top. Catal.* **56**, 1228 (2013).
[14] N. J. S. Costa, M. Guerrero, V. Collière, É. Teixeira-Neto, R. Landers, K. Philippot, L. M. Rossi. Organometallic preparation of Ni, Pd, and NiPd nanoparticles for the design of supported nanocatalysts. *ACS Catal.* **4**, 1735 (2014).
[15] P. M. Uberman, N. J. S. Costa, K. Philippot, R. C. Carmona, A. A. Dos Santos, L. M. Rossi. A recoverable Pd nanocatalyst for selective semi-hydrogenation of alkynes: hydrogenation of benzyl-propargylamines as a challenging model. *Green Chem.* **16**, 4566 (2014).
[16] M. A. S. Garcia, R. S. Heyder, K. C. B. Oliveira, J. C. S. Costa, P. Corio, E. V. Gusevskaya, E. N. dos Santos, R. C. Bazito, L. M. Rossi. Support functionalization with a phosphine-containing hyperbranched polymer: a strategy to enhance phosphine grafting and metal loading in a hydroformylation catalyst. *Chemcatchem* **8**, 1951 (2016).
[17] M. Ibrahim, M. A. S. Garcia, L. L. R. Vono, M. Guerrero, P. Lecante, L. M. Rossi, K. Philippot. Polymer versus phosphine stabilized Rh nanoparticles as components of supported catalysts: implication in the hydrogenation of cyclohexene model molecule. *Dalton Trans.* **45**, 17782 (2016).
[18] L. M. Rossi, I. M. Nangoi, N. J. S. Costa. Ligand-assisted preparation of palladium supported nanoparticles: a step toward size control. *Inorg. Chem.* **48**, 4640 (2009).
[19] C. A. Henriques, S. M. A. Pinto, J. Pina, C. Serpa, A. Fernandes, L. M. Rossi, M. F. Ribeiro, M. M. Pereira, M. J. F. Calvete. Cost-efficient method for unsymmetrical meso-aryl porphyrins and iron oxide-porphyrin hybrids prepared thereof. *Dalton Trans.* **45**, 16211 (2016).

[20] C. W. Liria, V. A. Ungaro, R. M. Fernandes, N. J. S. Costa, S. R. Marana, L. M. Rossi, M. Teresa Machini. Synthesis, properties, and application in peptide chemistry of a magnetically separable and reusable biocatalyst. *J. Nanopart. Res.* **16**, 2612 (2014).
[21] V. A. Ungaro, C. W. Liria, C. D. Romagna, N. J. S. Costa, K. Philippot, L. M. Rossi, M. Teresa Machini. A green route for the synthesis of a bitter-taste dipeptide combining biocatalysis, heterogeneous metal catalysis and magnetic nanoparticles. *Rsc Adv.* **5**, 36449 (2015).
[22] J. P. Cheng, R. Ma, M. Li, J. S. Wu, F. Liu, X. B. Zhang. Anatase nanocrystals coating on silica-coated magnetite: role of polyacrylic acid treatment and its photocatalytic properties. *Chem. Eng. J.* **210**, 80 (2012).
[23] F. Effenberger, R. A. Couto, P. K. Kiyohara, G. Machado, S. H. Masunaga, R. F. Jardim, L. M. Rossi. Economically attractive route for the preparation of high quality magnetic nanoparticles by the thermal decomposition of iron(III) acetylacetonate. *Nanotechnology* **28**, 115603 (2017).
[24] A. Bensalem, F. Bozon-Verduraz, M. Delamar, G. Bugli. Preparation and characterization of highly dispersed silica-supported ceria. *Appl. Catal. A Gen.* **121**, 81 (1995).
[25] P. Burroughs, A. Hamnett, A. F. Orchard, G. Thornton. Satellite structure in the X-ray photoelectron spectra of some binary and mixed oxides of lanthanum and cerium. *J. Chem. Soc. Dalton Trans.* **17**, 1686 (1976).
[26] J. El Fallah, L. Hilaire, M. Roméo, F. Le Normand. Effect of surface treatments, photon and electron impacts on the ceria 3d core level. *J. Electron Spectros. Relat. Phenomena* **73**, 89 (1995).
[27] S. Bagheri, N. Muhd Julkapli, S. Bee Abd Hamid. Titanium dioxide as a catalyst support in heterogeneous catalysis. *ScientificWorldJ* **2014**, 21 (2014).
[28] R. Güttel, M. Paul, F. Schuth. Activity improvement of gold yolk–shell catalysts for CO oxidation by doping with TiO_2. *Catal. Sci. Technol.* **1**, 65 (2011).
[29] K. Usha, B. Mondal, D. Sengupta, P. Kumbhakar. Photo-conversion efficiency measurement of dye-sensitized solar cell using nanocrystalline TiO_2 thin film as photo-anodes. *Measurement* **61**, 21 (2015).
[30] C. Liu, D. Yang, Y. Jiao, Y. Tian, Y. Wang, Z. Jiang. Biomimetic synthesis of TiO_2–SiO_2–Ag nanocomposites with enhanced visible-light photocatalytic activity. *ACS Appl. Mater. Interfaces* **5**, 3824 (2013).
[31] E. McCafferty, J. P. Wightman. Determination of the concentration of surface hydroxyl groups on metal oxide films by a quantitative XPS method. *Surf. Interface Anal.* **26**, 549 (1998).
[32] P. W. Park, J. S. Ledford. Effect of crystallinity on the photoreduction of cerium oxide: a Study of CeO_2 and Ce/Al_2O_3 catalysts. *Langmuir* **12**, 1794 (1996).